RSC Advances

ROYAL SOCIETY OF CHEMISTRY

www.rsc.org/advances

Color graphics

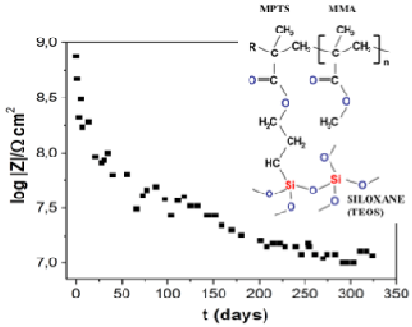

Novelty

Novel environmentally compliant Ce(IV) doped siloxane-PMMA coatings exhibiting dense cross-linked structure, high thermal stability, unique anticorrosive performance and self-healing ability.

Structural properties of cerium doped siloxane-PMMA hybrid coatings with high anticorrosive performance

S.V. Harb, F.C. dos Santos, B.L. Caetano, S.H. Pulcinelli, C.V. Santilli, P. Hammer

Instituto de Química, UNESP-Univ Estadual Paulista, 14800-900 Araraquara, SP, Brazil

Phone: ++55 16 3301 9887, Fax: ++55 16 3301 9692, e-mail address: peter@iq.unesp.br

This study reports on the characterization of cerium doped organic-inorganic hybrid coatings by correlating their structural properties with the corrosion protection efficiency of coated carbon steel. The films were prepared via the sol-gel route from radical polymerization of methyl methacrylate (MMA) with 3-methacryloxy propyltrimethoxysilane (MPTS) followed by acidic hydrolysis and condensation of tetraethoxysilane (TEOS). After identifying the optimum proportion of polymeric and silica phase for the formation of a highly ramified structure (MMA/TEOS = 4), increasing concentration of Ce(IV) ions (0.1% < Ce/Si < 5%) was added to the inorganic precursor to enhance the passivating character of the films. Nuclear magnetic resonance, X-ray photoelectron spectroscopy, small angle X-ray scattering, atomic force microcopy and thermogravimetry were used to characterize the structural properties and electrochemical impedance spectroscopy, potentiodynamic polarization curves and field emission scanning electron microscopy were employed to evaluate the corrosion resistance of the coated samples in standard saline environment. Structural analysis revealed a high degree of connectivity of the hybrid network, resulting in an enhanced thermal and electrochemical stability of the material. Detailed investigation of the structural effect of cerium species revealed that reduction of Ce(IV) ions during the polycondensation process catalyzes an increase of siloxane network connectivity (>87%) and enhances the polymerization of organic moieties. The electrochemical assays showed that the coatings posses an excellent long-term stability at high corrosion resistance of up to 10 GΩ cm^2 and current densities about 6 orders of magnitude lower than that of the bare carbon steel. For elevated Ce(IV) doping levels the self-healing ability was observed preventing during long-term exposure further progression of the corrosion process.

Keywords: Organic-inorganic hybrids, Structural properties, Corrosion protection, Cerium doping, Self-healing

1. Introduction

Organic-inorganic hybrids represent a new class of multifunctional materials, which combine the properties of the polymeric phase such as processibility, flexibility, transparency and tunable hydrophobicity with high mechanical, thermal and chemical stability of ceramic materials, such as silica or alumina. The interaction between organic and inorganic phases on the molecular scale can be of physical or chemical nature, the latter providing covalent bonds between both components. Hybrid nanocomposites can be easily prepared by different routes in a large number of possible combinations between the inorganic and organic components, resulting in a wide range of properties of the resulting material. This versatility provides a great potential for a number of applications such as sensors, optoelectronic systems, catalysts, biomaterials, drug delivery systems and protective coatings[1-4].

Especially in the important field of corrosion protection of metallic surfaces, hybrid coatings can be considered as environmentally compliant alternatives for current chromate based passivation methods, which suffer the drawback of containing toxic hexavalent chromium species. One of the most promising candidates for efficient corrosion protection is the siloxane-polymethyl methacrylate system (siloxane-PMMA), showing high transparency, chemical and thermal stability and mechanical strength[1,3,5]. Polymethyl methacrylate is a rigid, transparent, and colorless thermoplastic, well known as acrylic glass. The inclusion of an inorganic component such as silica into the PMMA matrix substantially improves its mechanical properties, thermal stability and adhesion to metallic substrates[3,6]. Recent studies have shown that siloxane-PMMA coatings, deposited on steel, exhibit excellent corrosion resistance both in saline and in saline/acidic medium[3,7]. Detailed analysis revealed that inorganic phase has an important role in promoting the adhesion between the film and metal substrate, while the organic phase hermetically seals the film structure. Thus the dense siloxane cross-link nodes interconnected covalently with short polymeric chains linked by the 3-methacryloxy propyltrimethoxysilane (MPTS) coupling agent, form a chemically inert barrier, which prevents the penetration of species that initiate corrosion process. In addition, these hybrid coatings exhibit hydrophobic character and as a consequence of their low intrinsic stress they can be prepared defect-free even with a thickness of several micrometers[3,7,8]. Some other features favor their use of among which can be highlighted the low costs of preparation, environmental compatibility, the versatility and the mild conditions of the sol-gel synthesis and low temperatures needed to cure the coatings. Consequently, siloxane-PMMA nanocomposite films prepared via sol-gel process posses a great

potential for large-scale application as environmentally compliant protection of metallic surfaces.

Several recent studies have reported an increase of the passivating character of hybrid coatings by the addition of species, which act as corrosion inhibitors. In particular, cerium IV and III ions have been identified as very effective, satisfying some basic requirements expected of a corrosion inhibitor such as: ability to increase the polycondensation degree of the siloxane network, to form insoluble hydroxides and oxides of low toxicity, besides its easy handling and availability[9]. The effects of low concentrations of cerium ions (<1000 ppm) in the structure of the hybrid has been investigated by some authors[9-11] including our group[12], showing for polysiloxane hybrids the active role of Ce(IV) in the formation of silanol radicals by reduction of Ce(IV) in the presence of ethanol resulting in an increase of the connectivity of the hybrid network and thus providing coatings of superior anticorrosive performance. Another interesting aspect, which can explain the prolonged durability of these coatings is the fact that introduced Ce ions form by redox reactions (Ce IV ↔ Ce III) insoluble oxides and hydroxides preferentially in the corrosion affected regions, leading to the currently much discussed "self-healing" effect[13-15].

Considering the great potential of cerium as corrosion inhibitor this work focuses on the structural investigation of Ce(IV) containing siloxane-PMMA hybrids used as corrosion resistant coatings on carbon steel. Based on the correlation of structural data with the corrosion protection efficiency first the most appropriate siloxane-PMMA matrix was identified[7], which was then used for addition of different amounts of Ce(IV). The structural properties of the siloxane-PMMA manocomposites were studied as a function of Ce(IV) concentration using ^{29}Si and ^{13}C nuclear magnetic resonance (NMR), X-ray photoelectron spectroscopy (XPS), small angle X-ray scattering (SAXS), atomic force microscopy (AFM) and thermogravimetry (TGA), while the corrosion protection efficiency was investigated by electrochemical impedance spectroscopy (EIS), potentiodynamic polarization curves and field emission scanning electron microscopy (FE SEM) after immersion of the samples in neutral saline solution (NaCl 3.5 %).

2. Experimental

The following commercially available reagents were used as received: tetraethylorthosilicate (TEOS), 3-methacryloxy propyltrimethoxy-silane (MPTS), methyl methacrylate (MMA), benzoyl peroxide (BPO), ethanol and tetrahydrofuran (THF), all acquired from Sigma-Aldrich. The MMA was

previously distillated to retire the inhibitor of polymerization. Cerium (IV) in form of ammonium ceric nitrate [$(NH_4)_2Ce(NO_3)_6$, Sigma-Aldrich] was used as Ce(IV) dopant.

The siloxane-polymethyl methacrylate hybrids were prepared using the sol-gel route in three stages: In the first step the MMA and the MPTS were copolymerized in THF using the thermal initiator (BPO) during 2 h at 70 °C under stirring in a reflux flask. Then, the inorganic component of the hybrid was prepared by hydrolysis and condensation of silicon alkoxide (TEOS). The hydrolysis of TEOS was carried in an ethanol solution by addition of acidified water (pH = 1) using nitric acid. Considered as the most suited precursor solution for the synthesis of corrosion protection coating, the sol containing a MMA to TEOS molar ratio of 4 (reference sample M4) and all other ratios were kept constant: H_2O/Si = 3.5, ethanol/H_2O = 0.5, BPO/MMA = 0.01 and TEOS/MPTS = 2 [3]. In a third step Ce(IV) was added in form of ammonium ceric nitrate $[(NH_4)_2Ce(NO_3)_6$ into the inorganic precursor using five different Ce/Si molar percentage: 0.1, 0.2, 0.3, 0.5, 0,7, 1, 3 and 5%, denoted as M4Ce_01, M4Ce_02, M4Ce_03, M4Ce_05, M4Ce_07, M4Ce_3, M4Ce_5, respectively. After 1 h of stirring at 25 °C in a closed flask, the suspension was mixed with the copolymer solution forming a homogeneous and transparent sol used for the film deposition. The following thermal cure (150 °C) ensured a high degree of polycondensation of the Ce(IV) modified hybrid structure.

For electrochemical corrosion tests, AFM, FE SEM and XPS measurements, coated A1010 carbon steel substrates (25 mm x 25 mm x 4 mm) were used, having a nominal composition (wt %) of C = 0.15%, Mn = 0.55 to 0.69%, Si = 0.13%, P = 0.03% and S = 0.01%, with the balance of Fe. The deposition of hybrid coatings was performed by dip-coating at a withdraw rate of 14 cm min^{-1}. Then the coated substrates were heated at 60 °C for 24 h and finally cured at 160 °C during 3 h. The coating thickness was determined by profilometry (Talystep, Taylor & Hobson). The adhesion of the films to the steel surface was evaluated by the ASTM D4541 method using a Posi-Test Pull-Off Adhesion Tester (De Felsko), determining the tensile pull-off force of detaching.

Unsupported hybrid films for NMR, XAS, SAXS and TGA analysis were obtained by drying and curing treatment of the sol in a Teflon dish. For NMR measurements the films were milled to obtain a powder. Solid-state ^{29}Si and ^{13}C magic-angle spinning nuclear magnetic resonance (MAS-NMR) spectra were recorded for powder samples using a VARIAN spectrometer operating at 300 MHz and 7.05 T. The Larmor frequency for ^{29}Si was 59.59 Hz. The spectra were obtained from the Fourier transformation of the free induction decays (FID), following a single $\pi/2$ excitation pulse and a dead

time of 2 s. Chemical shifts were referenced to tetramethylsilane (TMS), used as external standard. Proton decoupling was always used during acquisition of the spectra. Due to the high sensitivity of the NMR measurements, the uncertainty in the chemical shift values was less than 0.2 ppm.

The TG curves were recorded using a SDT Q600 (TA Instruments) thermal analysis system, with nitrogen as purge gas at a flow rate of 70 mL min^{-1}. About 7 mg of hybrid film was placed into alumina crucibles, and heated at a rate of 10 °C min^{-1} up to 600 °C.

The XPS analysis was carried out at a pressure of less than 10^{-7} Pa using a UNI-SPECS UHV instrument. The Mg Kα line was used (hν = 1253.6 eV) and the analyzer pass energy for the high-resolution spectra was set to 10 eV. The inelastic background of the Ce 3d spectra was subtracted using Shirley's method. Due to sample charging, the binding energy scale was corrected using the C 1s hydrocarbon component of the PMMA set to 285.0 eV. The composition was determined with an accuracy of ±10% from the ratio of the relative peak areas corrected sensitivity factors of the corresponding elements. The spectra were fitted without placing constraints using multiple Voigt profiles. The width at half maximum (FWHM) varied between 1.0 and 2.0 eV and the accuracy of the peak positions was ±0.1 eV.

The SAXS measurements were performed using the SAS 2 beam-line at the National Synchrotron Light Laboratory (LNLS) in Campinas, Brazil. An asymmetrically cut and bent Si(111) crystal was used to focus horizontally the monochromatic X-ray beam (λ = 0.1608 nm). The scattering intensity I(q), collected with a two-dimensional X-ray detector (Pilatus, 300k, 84 mm x 107 mm), was determined as a function of the modulus of the scattering wave vector $q = 4\pi/\lambda \sin\theta$, θ being half of the scattering angle.

Atomic force microscopy (AFM) measurements were carried out using the tapping mode of the Aglient 5500 instrument and field emission scanning electron microscopy (FE SEM) was performed using the FEI Inspect F50, installed at the Electron Microscopy Laboratory (LME) of the National Nanotechnology Laboratory (LNNano) in Campinas, Brazil.

The electrochemical measurements of coated and uncoated steel samples were carried out for different immersion periods at 25 °C in 80 mL of a naturally aerated 3.5% NaCl solution at room temperature. For electrochemical measurements an $Ag/AgCl/KCl_{sat}$ electrode, connected to the working solution through a Luggin capillary, was used as reference, and a Pt grid as the auxiliary

electrode. The working electrode was mounted in an electrochemical flat cell, exposing a geometric area of 1 cm^2 to the solution. Polarization curves were recorded after 4 h of immersion into the electrolyte using a potentiostat/galvanostat (EG&G Parc-273), in the overpotential range of -150 mV to +1000 mV versus the open circuit potential, E_{OC}, referred to the $Ag/AgCl/KCl_{sat}$ electrode, at a scan rate of 0.166 mV s^{-1}. The corrosion potentials and apparent corrosion current density values were directly estimated from classical *E* (mV) *vs. log i* (A cm^{-2}) curve. The polarization curves were qualitatively analyzed and only used to compare the coated materials with different formulation. The electrochemical impedance spectroscopy (EIS) measurements were performed after 1 day and for some chosen samples during 300 days of immersion in saline solutions using a Potentiostat/Galvanostat EG&G Parc-273 and a Frequency Response Analyzer Solartron-SI1255. The EIS tests were performed applying 10 mV (rms) to the E_{OC} value, starting from 10^5 to $5x10^{-3}$ Hz with 10 points/decade. For all samples, E_{OC} was measured for 1 h, then the E_{OC} value was applied for 15 min with simultaneous measuring of the current, which stabilized during this time, and finally the impedance spectra recorded. To guarantee the reproducibility of the results all electrochemical measurements were performed in duplicate.

3. Results and discussion

3.1 Structural analysis

Figure 1 displays a representative image of a siloxane-PMMA hybrid coated carbon steel (Fig. 1a) and the AFM surface morphology of sample M4Ce_07 containing 0.7% Ce (Fig. 1b). All films show a very smooth surface (R_{RMS} = 0.3 nm) without features, indicating the formation of a dense and compact layer. The thickness of the transparent coatings increased from about 1 μm to 1.8 μm with the cerium content, due to the slight viscosity increase of the precursor solution[10]. The tensile pull-off force of detaching was for all coatings higher than the 8 MPa, the limit of the Pull-Off Adhesion Tester, indicating a very good adhesion of the film to the substrate. This might be related with the strong interaction of the hydroxyl-rich oxide layer promoting a strong interaction between the steel substrate and the silanol groups of the inorganic part of the hybrid[16].

The polymerization degree of the methacryloxy groups was studied by ^{13}C solid state MAS-NMR, shown in Figure 2. The comparison of the hybrid spectra with resonance signals of MMA

evidenced the formation of a cross-linked organic phase, showing signals of quaternary carbon atoms (b'), C=O groups bonded to aliphatic carbon groups (c'), and aliphatic -CH2- groups (a')[3]. The absence of MMA signals at 125 ppm (a) and 137 ppm (b) for all samples, related to vinylic carbon atoms (C=C), and C=O groups bonded to these C atoms (c), evidenced the complete polymerization of acrylate monomer. Additionally, the small features, located at 12 ppm and 28 ppm, were identified as due to C-Si and C-C-C groups of MPTS, respectively[3].

The local bonding structure of the inorganic phase was studied by ^{29}Si nuclear resonance spectroscopy. Figure 3 shows the spectra of four chosen hybrid samples prepared with increasing Ce(IV)/Si molar percentage of 0% (M4), 0.1% (M4Ce_01), 0.5% (M4Ce_05) and 5% (M4Ce_5). The main spectral features are the broad resonance peaks at about -92, - 102 and -110 ppm, assigned to Q^2 ($Si(OSi)_2(OR)_2$), Q^3 ($Si(OSi)_3(OR)$) and Q^4 ($Si(OSi)_4$, R = H or CH_2CH_3) species, which are related to the polycondensation product of TEOS. Resonances related to MPTS polycondensation products, containing one non-hydrolysable Si-C bond, were observed at -44, -56 and -65 ppm, assigned to T^1 ($-CH_2Si(OSi)(OR)_2$, R = H or CH_3), T^2 ($-CH_2Si(OSi)_2(OR)$) and T^3 ($-CH_2Si(OSi)_3$) units[3,17]. The absence of monomer species T^0 ($-CH_2Si(OR)_3$) and Q^0 ($Si(OR)_4$) is in agreement with the cluster-cluster condensation mechanism, expected under strongly acid conditions[18]. The proportions of T^J and Q^J species present in the hybrid-nanocomposite were extracted from the spectra by a peak fitting procedure used to determine the relative peak area of each species. As expected, the intensity ratio of Q^J/T^J species was found to be close 2, in agreement with the proportions of the TEOS and MPTS precursors used in the synthesis. The polycondensation degree, C_d, of the inorganic phase was determined from the proportions of each T^J and Q^J species according to the equation: $C_d = [(T^1 + 2T^2 + 3T^3)/3 + (Q^1 + 2Q^2 + 3Q^3 + 4Q^4)/4] \times 100$.

The C_d values extracted from the spectra by fitted Voigt profiles are listed in Table 1. The results show a steep increase of connectivity of the inorganic phase from ~83% (M4 reference) to about 87% for the M4Ce_01 sample. With increasing cerium concentration the C_d values decrease below 80% (Table 1). The increase of the degree of polycondensation for low cerium doping levels can be related with the active role of Ce(IV) as very efficient oxidation agent, which enhances the polycondesation process by creation of silanol radicals, thus leading a higher network connectivity, as reported for polysiloxane hybrids[9,12]. However, as shown below, the lower polycondensation degree observed for cerium rich samples might come form an another effect, related with the increasing

formation of cerium oxide an hydroxide species. To elucidate this aspect the samples were analyzed using X-ray small angle X-ray scattering and by X-ray photoelectron spectroscopy.

Figure 4 displays the SAXS intensity profiles corresponding to siloxane-PMMA pallets with Ce/Si molar ratio between 0% and 1%. The scattering curves show a Gaussian decay for intermediate q-values and a plateau in the lower q-region, indicative for the Guinier regime[19]. This feature is generally observed for a biphasic system satisfying a two-electron density model in which a dilute set of non-interacting particles dispersed in a homogenous matrix. Considering for all samples a volume fraction of inorganic phase of less than 20% the scattering can be attributed to the siloxane nanoparticles embedded in the PMMA matrix[20]. The shift of the plateau to lower q-values with Ce/Si molar ratio up to 0.3 indicates that the siloxane nanoparticles increase in size. For higher cerium concentrations the saturation behavior suggests that additional cerium does not significantly influence the polycondensation process of the inorganic phase, in agreement with the lower C_d values observed by NMR.

To determine the average size of the siloxane scattering centers the Guinier equation was applied[19]: $I(q) = I(0) \exp(-(R_g q)^2/3)$ for $q \rightarrow 0$, where R_g is the Guinier average of the radius of gyration of the scattering particles and *I(0)*, the pre-exponential term. For two-electron density systems the pre-exponential is given by $I(0) = N(\Delta\rho)^2 \langle v^2 \rangle$, N being the specific number of particles, $\Delta\rho$ the difference in electron density between both phases and $\langle v^2 \rangle$ the average of the squared particle volume. A nearly linear dependency between ln(I(0)) and R_g^2 was observed as the Ce/Si molar ratio increases up to 0.3, indicating the invariance of *N and* $(\Delta\rho)$. Thus the observed R_g increase from about 0.8 nm (M4 reference) to about 2.3 nm (M4Ce_03) (inset of Fig. 4) could proceed through the cerium induced monomer accretion to individual siloxane cluster, rather than by cluster-cluster aggregation growth. Again, up to intermediate doping levels the observed dependence suggests a active role of Ce(IV) in the enhanced growth of a cross-linked siloxane phase, a result consistent with NMR data.

The quantitative XPS analysis confirmed the formation of polysiloxane hybrid films with a fixed fraction of the organic and inorganic phase, in good agreement with the nominal MMA/TEOS ratio of 4 (C: 55.0 at.%, O: 38.5 at.%, Si: 6.5 at.%). According to Table 1, the cerium concentration increased with the introduced quantity of Ce(IV) from a value below the detection limit (~0.05 at.%) to 1.1 at.%. It is important to note, that XPS spectra obtained for unsupported hybrid films, used for the

NMR, XAS, SAXS and thermal analyses, were identical with those obtained for films prepared by dip-coating.

The influence of Ce(IV) addition on the chemical bonding structure of the hybrid phase was investigated by the peak-form analysis of the Ce 3d to determine the degree of Ce(IV) reduction, which is expected to be indicative for Ce(IV) oxidation power in formation of silanol and metacrylate radicals during the polymerization process[9,12]. Figure 5 shows the Ce 3d spectra fitted using 5 spin-orbit doublets for the M4Ce_05, M4Ce_1 and M4Ce_5 samples and the Ce(IV) ammonium ceric nitrate salt reference. Being close to the detection limit, the deconvolution of noisy Ce 3d spectra of the sample with the lowest doping level (M4Ce_01) was not possible. The fitted components labeled v_i and u_i are due to corresponding $3d_{5/2}$ and $3d_{3/2}$ spin-orbit states, respectively. According to Reddy et al.[21] parts of the complex but distinct Ce 3d features are related to the final-state occupation of the Ce 4f level, resulting in shake-down satellites. The v_3/u_3 and v_1/u_1 doublets, separated by 18.6 eV, are due to primary photoemission from Ce(IV) and Ce(III) cations, respectively. The v/u and v_2/u_2 doublets are shake-down features resulting from the transfer of one or two electrons from a filled O 2p to an empty Ce 4f orbital during the Ce(IV) photoemission, and the v_0/u_0 doublets are related to the shake-down of Ce(III) cations.

It is well known that cerium species suffer an X-ray induced photo-redox process resulting in a partial conversion of Ce(IV) into Ce(III) and vice versa[12]. Therefore, to be able to follow the influence of the Ce(IV) oxidation agent on the phase formation process, identical irradiation dose an acquisition time was used for all photoemission experiments. The fitted spectrum of the ammonium ceric nitrate reference has shown that the X-ray induced reduction led to a Ce(IV) fraction of 76,4% (Fig. 5). Relative to this value the percentages of remaining Ce(IV), derived from relative Ce(IV) and Ce(III) sub-peak intensities, were lowest for hybrids with low cerium concentrations. For all hybrids, except M4Ce_01, the Ce(IV) percentages are listed in Table 1 and plotted in Figure 6 together with the NMR polycondensation degree (C_d) as a function of the Ce to Si molar percentage. The data show that relative to the ceric nitrate reference up to 62% of Ce(IV) was reduced to Ce(III) during the polycondensation and polymerization process of hybrids with low cerium content. Combining these results with NMR data it can be concluded that at low doping levels the presence Ce(IV) leads to an increase of the formation rate of silanol and methacrylate radicals which enhance the polycondensation reactions and the polymerization of organic moieties, thus leading to the formation of highly cross-

linked hybrid network. At elevated doping levels the influence of Ce(IV) on the kinetics of the phase formation is still present, however, the excess of the dopant leads to formation of cerium phases, such as which as oxides and hydroxides, which might have influence on the thermal and electrochemical characteristics of the material. Additionally, XPS results for cerium rich M4Ce_5 sample have shown traces of nitrogen in the form of nitrate (NO_3^-), located at N 1s binding energy of 407.5 eV, suggesting the presence of a small quantity of re-precipitated Ce salt.

Information on the thermal stability, related to the overall connectivity of the hybrid network, were obtained by thermogravimetric analysis. The differential curves (DTG), obtained in nitrogen atmosphere (Fig. 7), indicate the existence of four degradation stages of the siloxane-PMMA hybrid. The first three events (d_1, d_2 and d_3) are associated with the depolymerization of PMMA. The events at about 240 °C (d_1) and 310 °C (d_2) are associated with the rupture of the head-to-head segments and to unsaturated chain ends, while the event at 400 °C, corresponds to random scissions of the polymer chains[22,23]. The small event above at about 480 °C (d_4), can be attributed to the dehydration of silanol groups corresponding to T^1, T^2, Q^2 and Q^3 species present in the SiO_2 network[18]. Except for the M4Ce_5 sample the thermal stability of the hybrids is limited to about 200 °C. It is interesting to note, that relative to the M4 reference, the hybrids with lower cerium concentration exhibit a suppressed degradation rate for d_1 and d_2 events, most clearly visible for the M4Ce_01 sample. On the other hand, with increasing Ce content, a systematic shift of the d_3 event from 390 °C (M4) to temperatures up to 415 °C (M4Ce_5) occurs, indicating a higher thermal stability of the cerium rich phase against random depolymerization of the organic segments. Both effects evidence an overall cerium induced increase of the thermal stability. This effect is more evident for intermediate Ce/Si molar ratios, corresponding to an overall cerium doping level of about 500 ppm. Table 1 summarizes the relative intensities of d_1 and d_2 event relative to the M4 reference, together with the temperature of the T_3 event. Although the polycondensation degree of the M4Ce_07 sample is somewhat lower than the M4 reference decisive for the barrier propriety, discussed below, is the overall connectivity of the hybrid network. As can be observed in Table 1 the thermal stability against depolymerization of the M4Ce_07 sample is about 15 °C higher than for the M4 reference, indicating that hybrids in the intermediate cerium concentration range combine elevated inorganic network connectivity with a highly cross-linked structure. The DTG data are consistent with AFM, NMR and XPS results, indicating the formation of a compact and highly cross-linked structure with enhanced thermal stability.

3.2 Corrosion analysis

The electrochemical performance of hybrid coatings, containing increasing concentration of cerium, was evaluated using electrochemical impedance spectroscopy curves, recorded for different periods of immersion in saline solution (3.5% NaCl). Figure 8 displays the complex plane Nyquist and Bode plots for the M4 reference sample and cerium hybrid coatings after 1 day of immersion. Compared to bare steel, the coated samples show up to 6 orders of magnitude higher impedance modulus (Fig. 8b), reaching almost 10 GΩ cm^2 for the sample with intermediate cerium concentration (M4Ce_07). This values is about two orders of magnitude higher than the highest corrosion resistance reported for cerium doped polysiloxane hybrids[11,12,24] and higher than those recently reported for epoxy-silane coatings on Mg alloy, however using a 0.3% NaCl solution[25]. It should be noted, that this EIS performance, obtained for only 1-2 μm thick hybrid films, already approaches the behavior of high performance paints. Furthermore, it can be observed that at low frequencies the hybrid coatings containing intermediate cerium concentrations show a slightly better performance than the M4 reference, while the cerium rich samples display the highest Z modulus in the higher frequency range (1-10^5 Hz). The latter feature might be related to a passivation effect by of cerium oxide/hydroxide formation, a point that will be discussed below. For all samples the phase angle dependence (Fig. 5c) shows a broad band with nearly pure capacitive behavior ($\Phi < -80°$), which extends over almost five orders of magnitude (M4Ce_07), suggesting the presence of at least two time constants, one in the high frequency range of 1 – 10 kHz (HF), and the second in the low frequency interval (LF) of 1 – 10 Hz.

The electrical equivalent circuit used to fit the experimental data of M4Ce_05 and M4Ce_07 (inset of Table 2 and fits in Fig. 8), representative for all other samples, contains two time constants: R_2 and CPE_2 refer to the HF resistance and constant phase element for charge transfer in the surface region of the coating in contact with the solution, expected to act in the uptake process, while R_1 and CPE_1 are related to the LF resistive and capacitive response of the coating including the film/substrate interface[12]. In the case of the M4Ce_07 sample, the low frequency time constant is more evident, extending the broad phase angle band to lower frequencies. The derived model parameters are summarized in Table 2, showing for M4Ce_07 sample a slightly better performance than that found for the M4Ce_05 coating.

Despite the excellent EIS performance of the coatings observed after one day exposure, a more important aspect is whether the high corrosion resistance can be maintained during long time periods,

thus providing an applicable system for efficient corrosion protection of metallic surfaces. The immersion time dependence of the sample M4Ce_07, presented in Figure 9, evidences the high protection efficiency of the coating maintaining the impedance modulus above $10^8\ \Omega\ cm^2$ for more than 10 months contact with the saline environment (Fig. 9b). With increasing exposure time the LF time constant is shifted towards higher frequencies close to that observed for bare steel (~10 Hz). Although after 10 months of exposure the impedance value is still four orders of magnitude higher than that of bare steel, this shift indicates the beginning of a corrosion progress at the film/steel interface.

To analyze the aging process of the samples in more detail, the time dependence of the elements of the equivalent circuit was determined and plotted in Figure 10. For the studied sample (M4Ce_07), a small but continuous decrease of the resistance values and a increase of the constant phase element can be observed. While the double layer capacitance CPE_2 increases by a factor of 5, the coating capacitance CPE_1 only by a factor 1.4. Compared with a conventional capacitor having a CPE exponent of n = 1, an exponent of n = 0.5 is associated with a diffusion process through film pores[26]. Values in the intermediate range $0.5 < n < 1$ are related to coating roughness and inhomogeneous current distribution. As the CPE exponent for the high frequency time constant (R_2/CPE_2) decreases from 0.87 to 0.66, while for the low frequency time constant (R_1/CPE_1) only from 0.97 to 0.95 (Table 2), it can be concluded that the reduced corrosion resistance of the M4_07 coating after long-term exposure is primarily caused by a continuous increase of the porosity of the near surface region of the coating.

The high surface roughness of the coating and the beginning corrosion process at the film/steel interface was evidenced by the inspection of the surface by FE SEM, which showed after 328 days contact with the electrolyte the formation of several micro-pits, with a size of about 250 nm (Fig. 11). The maximum period of stability, defined as time interval before suffering an impedance drop of about 2 - 4 orders of magnitude, are listed in Table 1 for all samples. The values indicate a tendency of elevated anticorrosive stability for coatings in the intermediate cerium concentration range. It should be pointed out that to best of authors' knowledge this long-term performance at elevated impedance values was not yet reported for protective coatings with micrometric thickness.

Although samples with higher cerium concentrations were less stable in chloride solution than those in the intermediate concentration range, another interesting time-dependence was observed, which can be directly related to the self-healing effect of cerium[13-15]. In contrast to samples with low cerium content, M4Ce_3 and M4Ce_5 showed after a local failure of the coating only an impedance

drop of about two orders of magnitude and than remained stable at about 10^7 Ω cm^2. This time dependence, shown in Figure 12 for the coating M4Ce_5, is related to the presence of insoluble cerium oxides and hydroxides[12,14,27], preferentially formed in pits by the reaction of Ce^{3+} and Ce^{4+} with residual hydroxyl groups of the hybrid, according to equations 1 – 4. Evidence for the presence of oxides and hydroxides in cerium-rich films comes from the analysis of the XPS O1s spectra. For sample M4Ce_5 the spectral components of Figure 13 show a clear presence of cerium oxide (Ce-OH) and cerium dioxide (Ce-O) phases in the low binding energy tail of the spectum[28]. The three principals spectral components are related to bonding environments of oxygen present in the acrylic (O-C=O and O=C) and siloxane (O-Si) part of the hybrid[28].

$$Ce^{3+} + 3OH^- \leftrightarrows Ce(OH)_3 \quad (1)$$

$$2Ce(OH)_3 \leftrightarrows Ce_2OH_3 + 3H_2O \quad (2)$$

$$Ce^{3+} + 4OH^- \leftrightarrows Ce(OH)_4 \quad (3)$$

$$Ce(OH)_4 \leftrightarrows CeO_2 + 2H_2O \quad (4)$$

The excellent corrosion protection efficiency in saline medium of Ce(IV) doped hybrid coatings was confirmed by the comparison of the potentiodynamic polarization curves with the M4 reference, displayed in Figure 14. All coatings show very low current densities and overpotential stability up to 1 V, corresponding to electrical field of about 10^6 V/m. While the current density of the M4 reference in saline medium is about 5 orders of magnitude lower than that of bare steel, samples with intermediate Ce content exhibit even lower current densities approaching 10^{-11} A cm^{-2}. To compare the polarization results with those obtained by impedance spectroscopy, the polarization resistances (R_p) were calculated from Tafel curves. As expected, the values were close to those determined by EIS. In the case of sample M4Ce_07 the polarization resistance obtained by EIS was $5x10^9$ Ω, while from polarization curve a value of $2x10^9$ Ω was calculated.

The combination of high impedance modulus and low current densities, even for high anodic potentials, allied with a long-term stability in saline medium are indicative for the exceptional performance of cerium doped siloxane-PMMA protective coatings. According to the electrochemical results, the performance of the coated samples in neutral saline medium can be established in the following cerium concentrations sequence: medium Ce > low Ce > high Ce >> bare steel. The superior performance at medium Ce concentrations can be related to the interplay of two beneficial effects:

higher network connectivity, induced the Ce(IV) oxidation agent, and beginning formation of cerium oxide and hydroxide species, which restore the film functionality as inert diffusion barrier against the corrosive attack. Although it is evident that self-healing is more effective for coatings with elevated cerium content. The correlation of NMR, SAXS and XPS results allowed to prove that the Ce(IV) induced formation of silanol radicals increases the polycondensation degree of the inorganic backbone and the polymerization of the organic moieties, thus leading to the formation of a dense hybrid network with enhances thermal stability and elevated barrier capability. Based on these results, cerium doped siloxane-PMMA coatings, prepared via sol-gel process with a thickness of several micrometers, can be considered as very promising candidates for "green" high performance protective coatings.

4. Conclusions

Smooth, defect-free, adherent and optically transparent siloxane-polymethyl methacrylate hybrid coatings containing different quantities of Ce(IV) were deposited onto carbon steel from sol prepared by acid-catalyzed hydrolytic polycondensation of TEOS and MPTS and radical polymerization of MMA.

NMR and SAXS results have revealed the active role of Ce(IV) in enhancing the polycondensation of the siloxane phase, leading to a highly ramified structure of nanometric siloxane cross-link nodes with connectivity up to 87%. The correlation of XPS and NMR data evidenced that the increase of the condensation degree is directly related to the degree of Ce(IV) reduction, both decreasing with increasing cerium concentration. Results of thermogravimetric analysis have shown that incorporation of Ce(IV) increases the thermal stability of the hybrids, an effect which can related to the enhancement of the overall connectivity of the network, induced by the enhanced hybridization of organic and inorganic moieties.

As a result, the cerium containing coatings show a superior corrosion protection performance than the undoped reference hybrid in neutral saline media. The combination of high impedance modulus ($>10^9\ \Omega\ cm^2$), overpotential stability at low current densities ($<10^{-11}$ A), and elevated long-term stability (up to 304 days), observed for coatings with intermediate cerium content, are consequences of a synergy effect of Ce(IV) induced densification process and formation of insoluble cerium species, which induce a self-healing effect in corrosion zones, thus increasing significantly the

lifetime of the coatings. Consequently, these Ce doped siloxane-PMMA thin films have a great potential as novel system for environmentally compliant corrosion protection of metallic surfaces.

Acknowledgements

We are grateful to FAPESP, CNPq and CAPES for the finacial support and to National Laboratory of Synchrotron Light Source for the SAXS and LME microscopy facilities.

References

1 C. Sanchez, P. Belleville, M. Popall, L. Nicole, Chemical Society Reviews, 2011, **40**, 696.

2 E. F. Molina, L. Marcal, H.W. Perreira de Carvalho, E.J. Nassar, K.J. Ciuffi, Polymer Chemistry, 2013, **4**, 1575.

3 V.H.V. Sarmento VHV, M.G. Schiavetto, P. Hammer, A.V. Benedetti, C.S. Fugivara, P.H. Suegama, S.H. Pulcinelli, C.V. Santilli, Surface & Coatings Technology, 2010, **204**, 2689.

4 C.V. Santilli, L.A. Chiavacci, L. Lopes, S.H. Pulcinelli, A.G. Oliveira, Chemistry of Materials, 2009, **21,** 463.

5 D.A. López, N.C. Rosero-Navarro, J. Bellarre, A. Duran, M Aparicio, S. Ceré, Surface & Coatings Technology, 2008, **202**, 2194.

6 F. Hammeri, I. Rozes, C. Sanchez, E. Le Bourhis, Journal of Sol-Gel Science and Technology, 2003, **26**, 413.

7 P. Hammer, F. C. dos Santos, B. M. Cerrutti, S. H. Pulcinelli, C. V. Santilli, Journal of Sol-Gel Science and Technology, 2012, **63**, 266.

8 P. Hammer, F.C. dos Santos, B.M. Cerrutti, S.H. Pulcinelli, C.V. Santilli, Progress in Organic Coatings, 2013, **76**, 601.

9 P.H. Suegama, H.G. de Melo, A. V. Benedtti, I.V. Aoki, Electrochimica Acta, 2009, **54**, 2655.

10 J.B. Cambon, F. Ansart, J.-P. Bonino, V. Turq, Progress in Organic Coatings, 2012, **75**, 486.

11 R.Z. Zand, K. Verbeken, A. Adriaens, Progress in Organic Coatings, 2012, **75**, 463.

12 P. Hammer, M.G. Schiavetto, F.C. dos Santos, S.H. Pulcinelli, A.V. Benedetti, C.V. Santilli, Journal of Non-Crystaline Solids, 2010, **356**, 2606.

13 M.F. Montemor, Surface & Coatings Technology, 2014, **258**, 17.

14 F. Zanotto, V. Grassi, A. Frignani, F. Zucchi, Materials Chemistry and Physics, 2011, **129**, 1.

15 M. L. Zheludkevich, J. Tedim, C. S. R. Freire, S. C. M. Fernandes, S. Kallip, A. Lisenkov, A. Gandini, M. G. S. Ferreira, Journal of Material Chemistry, 2011, **21**, 4805.

16 A.P. Romano, M. Fedel, F. Deflorian, M.G. Olivier, Progress in Organic Coatings, 2011, **72**, 695.

17 L. Fedrizzi, F.J. Rodriguez, S. Rossi, F. Deflorian, R. Di Maggio, Electrochimca Acta, 2001, **46**, 3715.

18 Y.H. Han, A. Taylor, M.D. Mantle, K.M. Knowles, Journal of Sol–Gel Science and Technolology, 2007, **43**, 111.

19 A. Guinier, (1964). Théorie et Téchnique de la Radiocristallographie. Paris: Dunod.

20 V. H. V. Sarmento, K. Dahmouche, C. V. Santilli, S. H.Pulcinelli and A. F. Craievich Journal of Applied Crystalography 2003, **23**, 473.

21 B.M. Reddy, Y. Yamada, T. Kobayashi, S. Loridant, J.C. Volta, Journal of Physical Chemistry B, 2003, **107**, 5162.

22 L.E. Manring, Macromolecules, 1989, **22**, 2673.

23 H.W.P. Carvalho, A.F. Suzana, C.V. Santilli, S.H. Pulcinelli, Polymer Engineering and Science, 2013, **53**, 1253.

24 S. Kozhukharov, V. Kozhukharov, M. Schem, M. Aslan, M. Wittmar, A. Wittmar, M. Veith, Progress in Organic Coatings, 2012, **73**, 95.

25 F. Brusciotti, D.V. Snihirova, H. Xue, M.F. Montemor, S.V. Lamaka, M.G.S. Ferreira, Corrosion Science, 2013, **67**, 82.

26 M.E. Orazem, B. Tribollet, Eds., *Electrochemical Impedance Spectroscopy*, 1st ed.; John Wiley & Sons, Inc.: Hoboken", page 12.

27 A. Pepe, M. Aparicio, S. Cere, A. Duran, Journal of Non-Crystalline Solids, 2004, **348**, 161.

28 AV. Naumkin, A. Kraut-Vass, S.W. Gaarenstroom, C.J. Powell, NIST X-ray Photoelctron Spectroscopy Database, Standard Reference Database 20, v. 4.1: htttp://srdata.nist.gov/XPS/

Tables

Table 1: Structural and electrochemical properties of Ce(IV) doped siloxane-PMMA hybrids: polycondensation degree C_d, determined by NMR; Ce concentration and Ce(IV) percentage, obtained by XPS; Relative intensity of d_1, d_2 and temperature of the d_3 event, obtained by TG; and maximum corrosion stability of coatings, determined by EIS in duplicate.

		Ce(IV) doped hybrids						
	M4 ref.	M4Ce_01	M4Ce_03	M4Ce_05	M4Ce_07	M4Ce_1	M4Ce_3	M4Ce_5
NMR C_d (%)*	82.8	87.1	83.6	82.7	79.3	78.5	77.6	77.3
XPS Ce conc. (at.%)**	-	***	< 0.1	0.1	0.15	0.2	0.4	1.1
XPS Ce(IV) fraction (%)	-	***	28.5±4	37.2±3	46.4±2.5	48.5±2.5	55.5±2	60.4±1.5
DTG events								
d_1 intensity	ref.	weak	weak	weak	weak	weak	weak	weak
d_2 intensity	ref.	weak	equal M4	equal M4	strong	strong	strong	strong
d_3 (°C)	390	395	395	398	405	408	410	415
EIS max. stability (days)	42	85	96	-	304	65	48****	304****

*Error: ±1.0. **Error: ±5%. *** below the XPS detection limit. ****Stabilization by self-healing

Table 2: Parameters of the electrical equivalent circuit (inset) for sample M4Ce_05 and M4Ce_07 determined after 1 day and 304 days (M4Ce_07) immersion in neutral 3.5% NaCl solution.

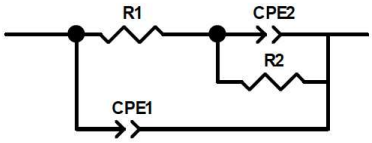

Sample	M4Ce_05 (1 day)		M4Ce_07 (1 day)		M4Ce_07 (304 days)	
χ^2	0.84×10^{-3}		0.69×10^{-3}		1.3×10^{-4}	
R_1 (Ω cm^2)	2.87×10^{7}	(7.00)*	5.77×10^{7}	(8.69)	6.13×10^{6}	(8.8)
CPE_1 (F cm^{-2} s^{n-1})	4.59×10^{-9}	(0.94)	3.88×10^{-10}	(3.88)	2.30×10^{-9}	(0.83)
n_1	0.59	(1.46)	0.97	(0.66)	0.95	(0.09)
R_2 (Ω cm^2)	8.33×10^{8}	(3.64)	5.49×10^{9}	(0.70)	3.42×10^{8}	(1.29)
CPE_2 (F cm^{-2} s^{n-1})	3.14×10^{-9}	(0.90)	1.71×10^{-9}	(0.88)	1.71×10^{-9}	(1.63)
n_2	0.96	(0.11)	0.87	(0.11)	0.66	(0.62)

*Error (%)

Figure captions

Fig. 1 a) Representative image of M4Ce_07 siloxane-PMMA hybrid coated carbon steel (A1010), and b) AFM topography of the sample.

Fig. 2 ^{13}C MAS/NMR spectra of hybrids prepared at a ratio MMA/MPTS = 4 and Ce/Si molar percentages of 0% (M4), 0.1% (M4Ce_01), 0.5% (M4Ce_05), 1% (M4Ce_1) and 5% (M4Ce_5). (The peak "s" refers to the chloroform solvent of MMA.) The inset shows the molecular structure of MMA and PMMA.

Fig. 3 ^{29}Si NMR spectra of hybrids prepared at a ratio MMA/MPTS = 4 and Ce/Si molar percentages of 0% (M4), 0.1% (M4Ce_01), 1% (M4Ce_1) and 5% (M4Ce_5).

Fig. 4 SAXS intensity profiles (I(q)) and Guinier radius of gyration R_g (insert) of hybrids prepared at a ratio MMA/MPTS = 4 and Ce/Si molar percentages between 0% (M4) and 1% (M4Ce_1). (The dashed line for R_g in the inset is a guide for the eye).

Fig. 5 Deconvoluted XPS Ce 3d spectra of Ce(IV) doped hybrids prepared at a ratio MMA/MPTS = 4 and Ce/Si molar percentages of 0.5% (M4Ce_05), 1% (M4Ce_1) and 5% (M4Ce_5), including the fitted spectrum ammonium ceric nitrate dopant ($(NH_4)_2Ce(NO_3)_6$).

Fig. 6 Correlation between the percentage of the Ce(IV) oxidation state %Ce(IV) and the polycondensation degree C_d as a function of the molar Ce/Si percentage, determined from de fitted XPS Ce 3d and ^{29}Si NMR spectra, respectively. (The dashed lines are guides for the eye).

Fig. 7 DTG and TG (insert) curves obtained for hybrids prepared at a ratio MMA/MPTS = 4 and Ce/Si molar percentages of 0% (M4), 0.1% (M4Ce_01), 0.5% (M4Ce_05), 1% (M4Ce_1) and 5% (M4Ce_5),

Fig. 8 Complex plane impedance (a), modulus impedance (b) and phase (c) plots of bare carbon steel and hybrid coatings prepared at a ratio MMA/MPTS = 4 and Ce/Si molar percentages between 0% (M4) and 5% (M4Ce_5), after 1 day exposure to unstirred and naturally aerated 3.5 % NaCl solution. (The solid lines are fits according the equivalent circuit, shown in the insert of Table 2, for M4_Ce05 and M4_Ce07 coated samples).

Fig. 9 Complex plane impedance (a), modulus impedance (b) and phase (c) plots of the M4Ce_07

hybrid coating prepared at a ratio MMA/MPTS = 4 and Ce/Si molar percentage of 0.7%, after exposure of up to 304 days in unstirred and naturally aerated 3.5% NaCl solution. (The solid line fits the data for 1 day exposure, according the equivalent circuit, shown in the inset of Table 2).

Fig. 10 Time dependence of resistances R_1, R_2 and constant phase elements CPE_1, CPE_2 of the equivalent circuit (inset Table 2) determined for the M4Ce_07 hybrid in 3.5% NaCl solution.

Fig. 11 FE SEM image of the M4Ce_5 coating after up to 328 days exposure in unstirred and naturally aerated 3.5% NaCl solution, showing localized pits of about 250 nm (arrows).

Fig. 12 Time dependence of the impedance modulus (M4Ce_5), showing a stabilization at about 10^7 Ω cm^2, indicative for the cerium induced self-healing effect of the coating.

Fig. 13 Deconvoluted XPS O 1s spectra of Ce(IV) doped hybrids prepared at a ratio MMA/MPTS = 4 and Ce/Si molar percentages of 1% (M4Ce_1), 3% (M4Ce_3) and 5% (M4Ce_5).

Fig. 14 Potentiodynamic polarization curves of bare carbon steel and hybrid coatings prepared at a ratio MMA/MPTS = 4 and Ce/Si molar percentages between 0% (M4) and 5% (M4Ce_5), recorded after 2 h of immersion in a) unstirred and naturally aerated 3.5% NaCl solution.

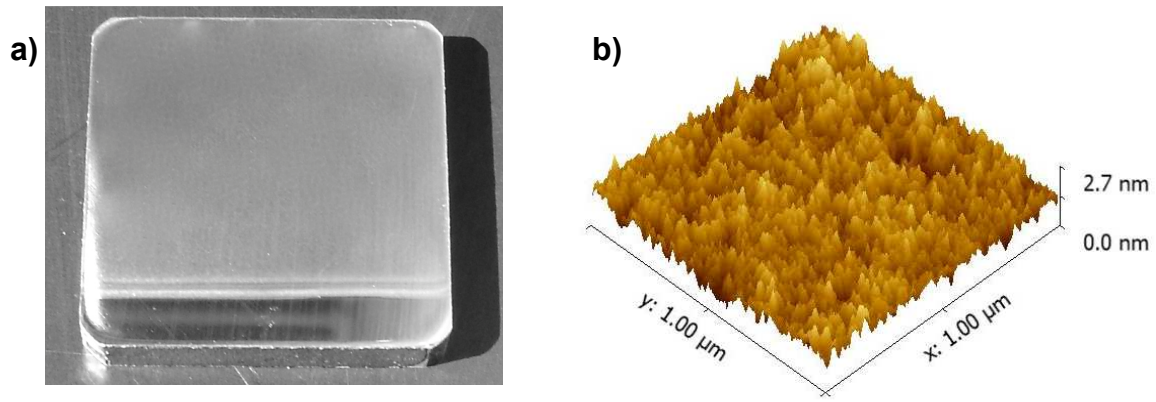

Fig. 1 Vargas et al.

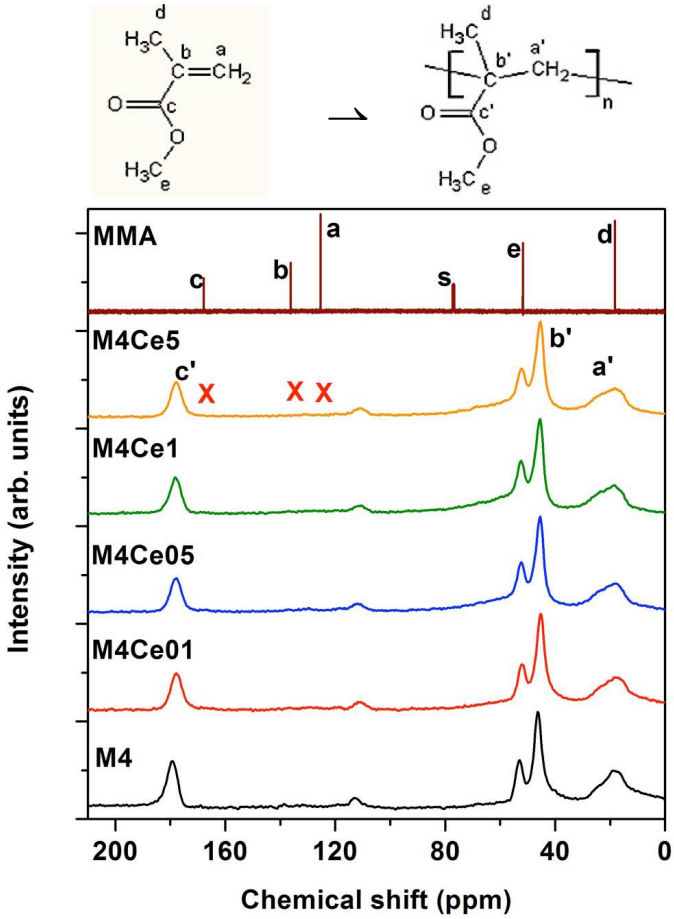

Fig. 2 Vargas et al.

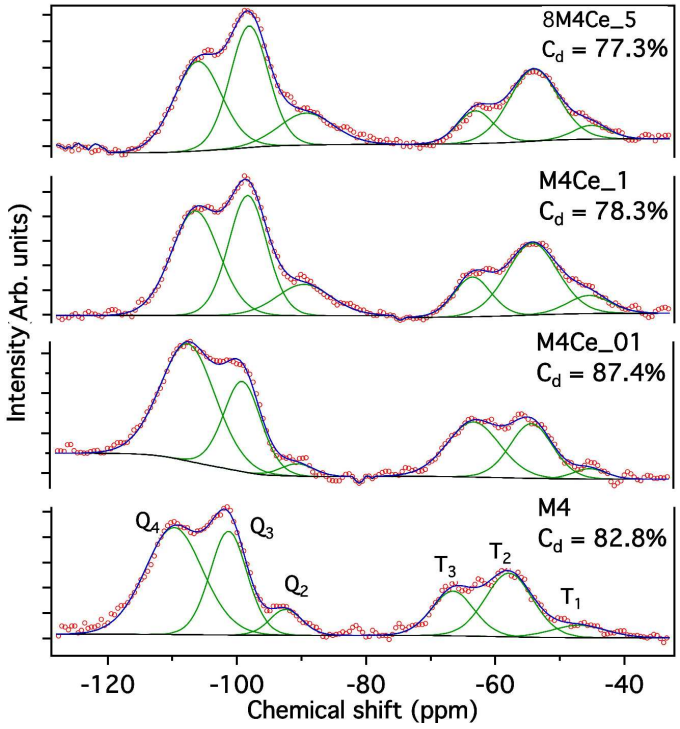

Fig. 3 Vargas et al.

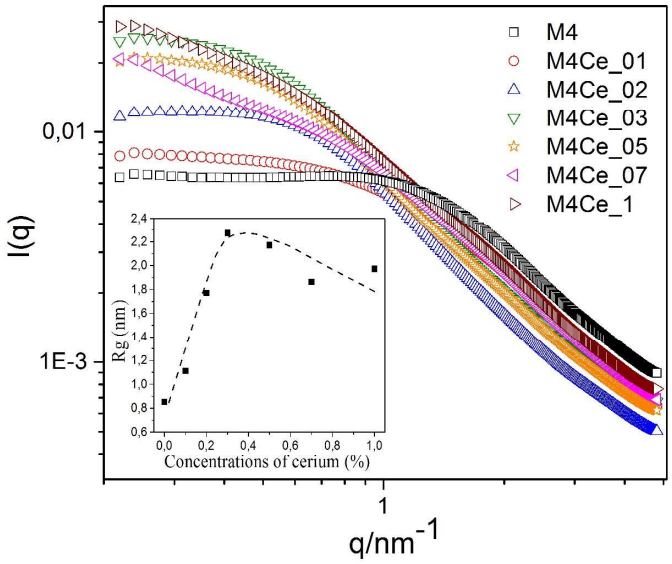

Fig. 4 Vargas et al.

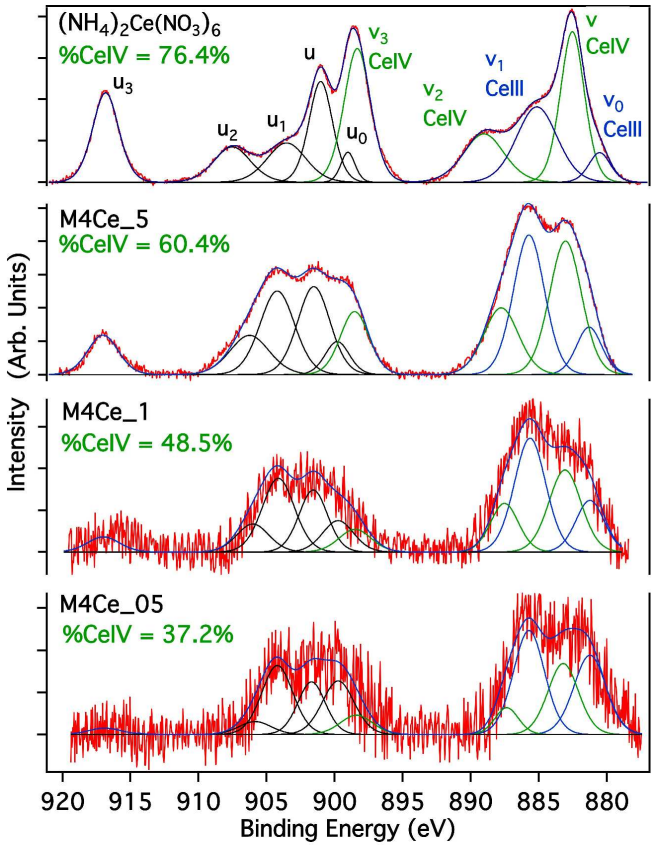

Fig. 5 Vargas et al.

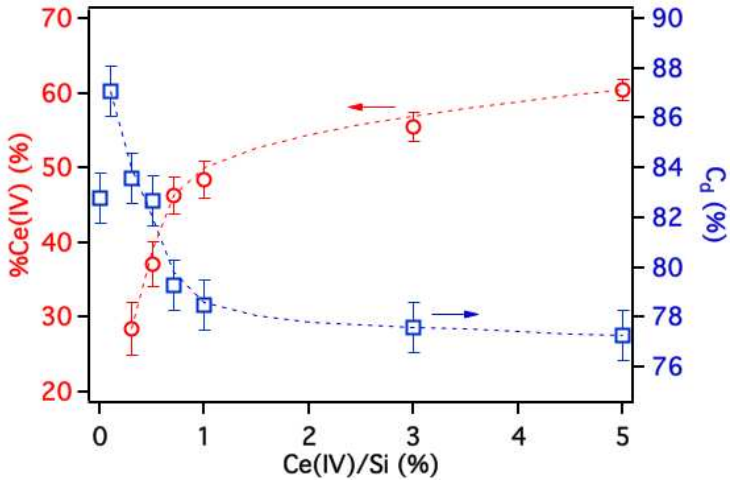

Fig. 6 Vargas et al.

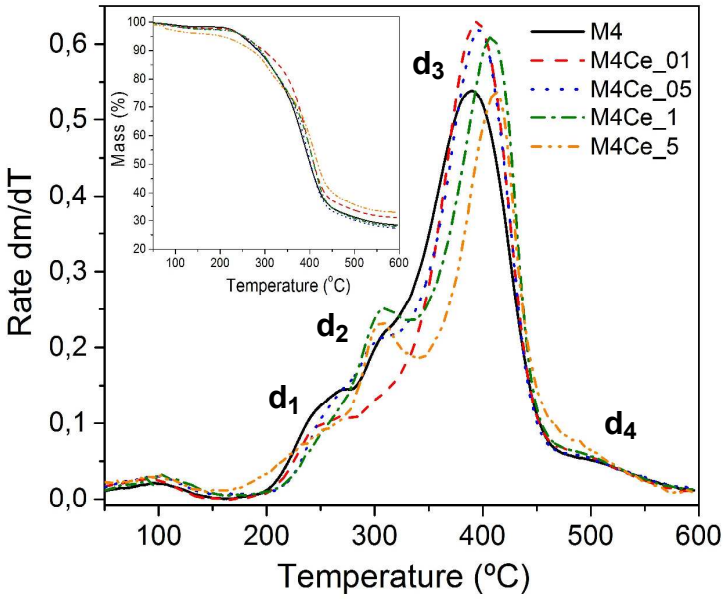

Fig. 7 Vargas et al.

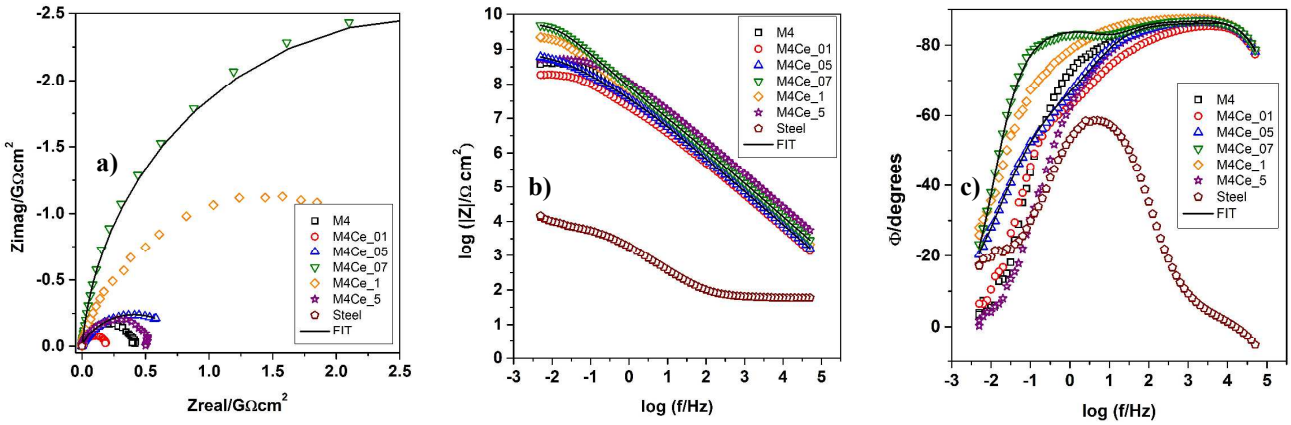

Fig. 8 Vargas et al.

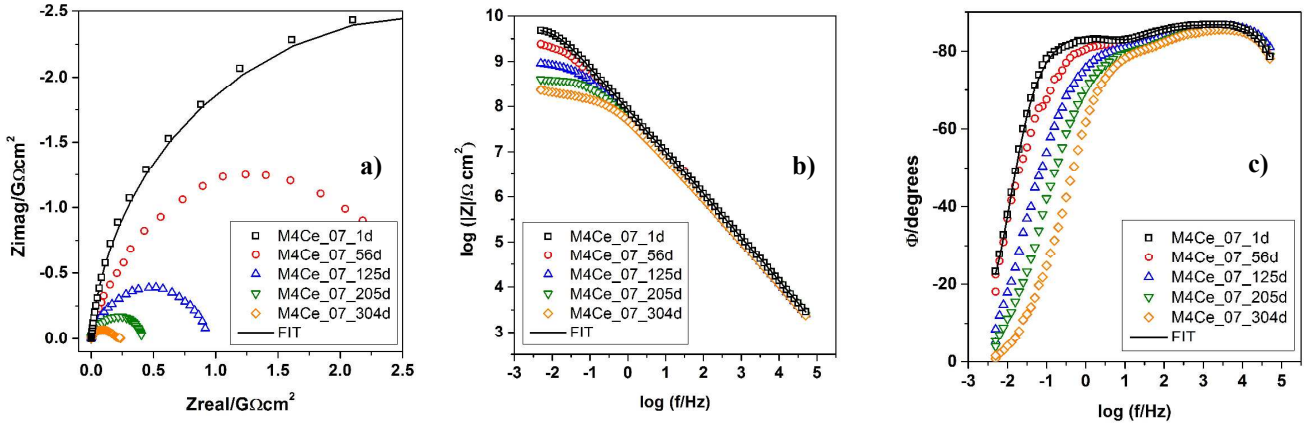

Fig. 9 Vargas et al.

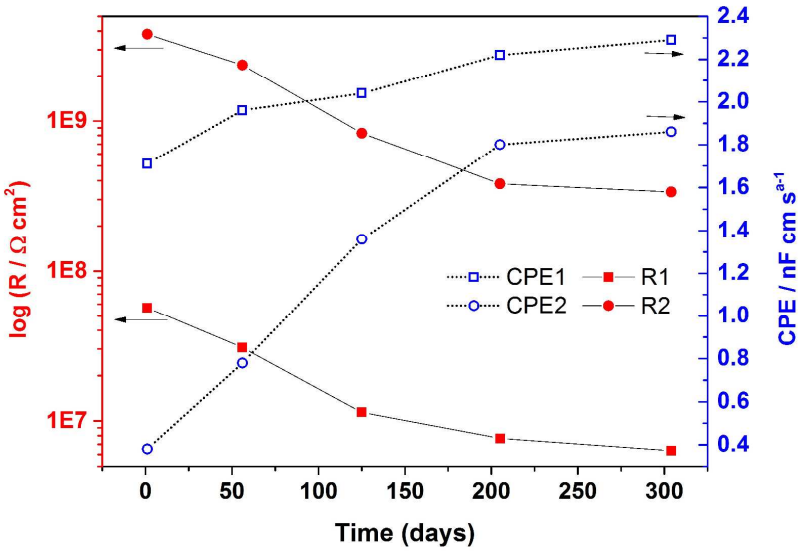

Fig. 10 Vargas et al.

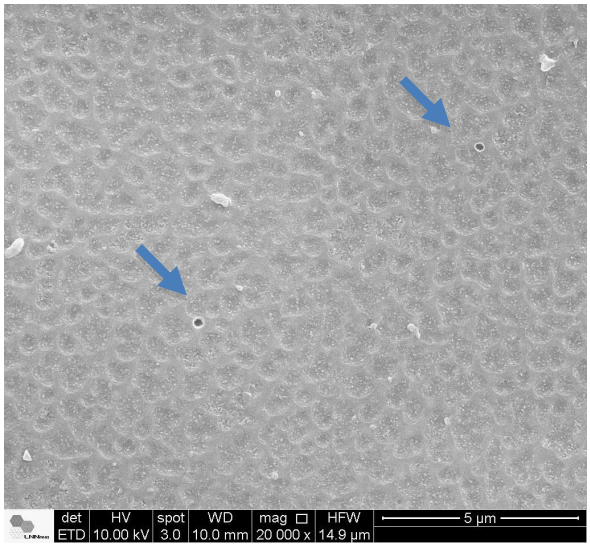

Fig. 11 Vargas et al.

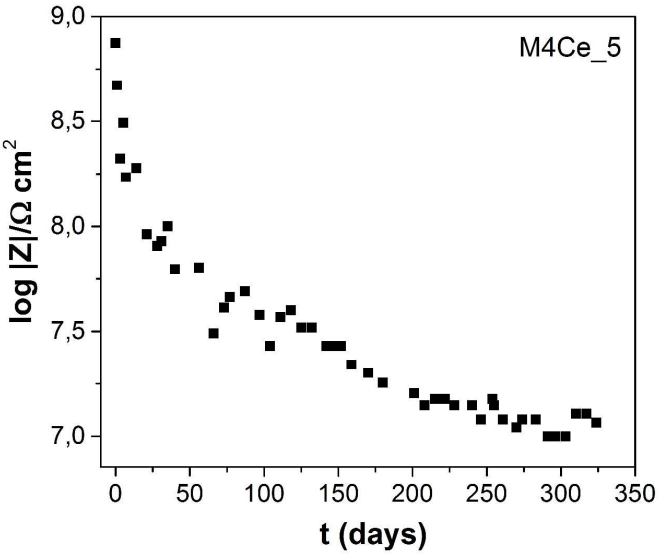

Fig. 12 Vargas et al.

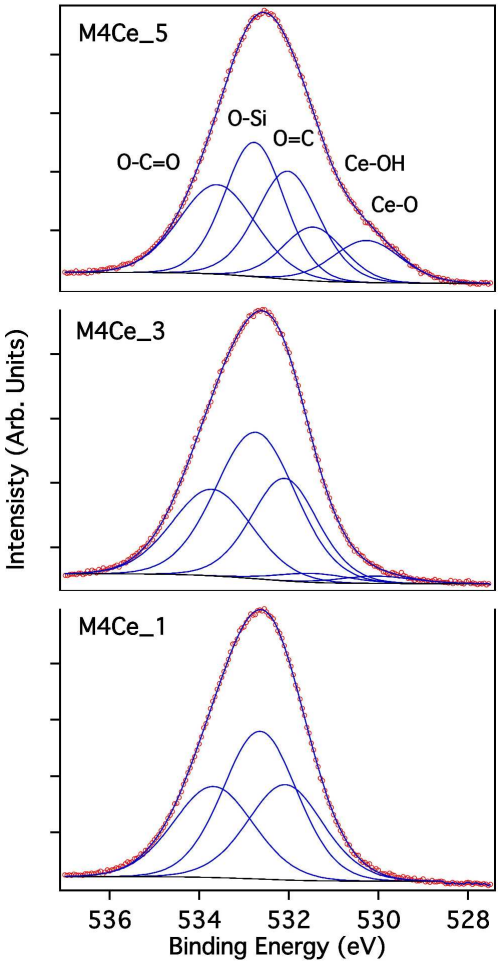

Fig. 13 Vargas et al.

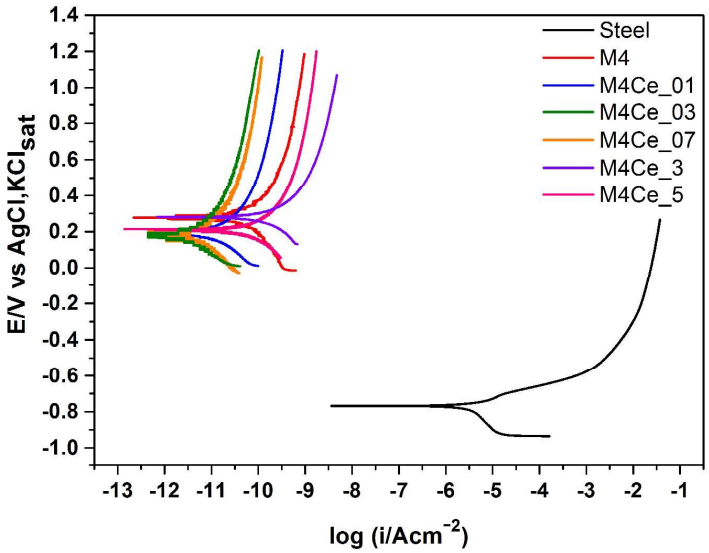

Fig. 14 Vargas et al.